Multiaxial pulsatile dynamics of the thoracic aorta and impact of thoracic endovascular repair

Ga-Young Suh [a,b,]*, Johan Bondesson [c], Yufei D. Zhu [b], Jason T. Lee [b], Michael D. Dake [d], Christopher P. Cheng [b]

[a] *Department of Biomedical Engineering, California State University, Long Beach: 1250 Bellflower Blvd, Long Beach, CA, 90840, USA*
[b] *Department of Vascular Surgery, Stanford University, 300 Pasteur Drive, Stanford, CA, 94305, USA*
[c] *Division of Dynamics, Chalmers University of Technology, SE-412 96, Gothenburg, Sweden*
[d] *Department of Cardiothoracic Surgery, Stanford University, 300 Pasteur Drive, Stanford, CA, 94305, USA*

HIGHLIGHTS

- Altered motion of the thoracic aorta after thoracic endovascular aortic repair.
- Geometric analysis with cardiac-gated computed tomography and computer modeling.
- Decreased motion of the stented aorta and increased motion above the stented aorta.
- Longitudinal curvature and diametric deformation affected by presence of endograft.

ARTICLE INFO

ABSTRACT

Purpose: The thoracic aorta is a highly mobile organ whose dynamics are altered by thoracic endovascular aorta repair (TEVAR). The aim of this study was to quantify cardiac pulsatility-induced multi-axial deformation of the thoracic aorta before and after descending aortic TEVAR.
Methods: Eleven TEVAR patients (8 males and 3 females, age 57–89) underwent retrospective cardiac-gated CT angiography before and after TEVAR. 3D geometric models of the thoracic aorta were constructed, and lumen centerlines, inner and outer surface curves, and cross-sections were extracted to measure aortic arclength, centerline, inner surface, and outer surface longitudinal curvatures, as well as cross-sectional effective diameter and eccentricity for the ascending and stented aortic portions.
Results: From pre- to post-TEVAR, arclength deformation was increased at the ascending aorta from 5.9 ± 3.1 % to 8.8 ± 4.4 % ($P < 0.05$), and decreased at the stented aorta from 7.5 ± 5.1 % to 2.7 ± 2.5 % ($P < 0.05$). Longitudinal curvature and diametric deformations were reduced at the stented aorta. Centerline curvature, inner surface curvature, and cross-sectional eccentricity deformations were increased at the distal ascending aorta.
Conclusions: Deformations were reduced in the stented thoracic aorta after TEVAR, but increased in the ascending aorta near the aortic arch, possibly as a compensatory mechanism to maintain overall thoracic compliance in the presence of reduced deformation in the stiffened stented aorta.

1. Introduction

While thoracic endovascular aortic repair (TEVAR) is increasingly employed to treat thoracic aortic dissections and aneurysms, long-term clinical and mechanical performance in the environment of the dynamic aorta is of rising concern. The thoracic aorta is directly connected to the dynamic heart, and undergoes displacement- and hemodynamically-induced cyclic loads in the longitudinal, bending, and cross-sectional directions. Implantation of TEVAR endografts changes the conformation and compliance of the repaired aorta, altering the geometry and dynamic motion of the implanted region as well as adjacent regions of the aorta. Such alterations may impact the short and long term evolution

---

of stent fracture, graft fatigue, thrombosis, in-stent restenosis, and downstream aortic diseases [1–4].

Despite the concern of possible complications, cardiac pulsatility-induced motion of thoracic aorta and its changes from pre-TEVAR to post-TEVAR state is not thoroughly understood. Previous studies have reported complex deformations and displacements of the thoracic aorta in healthy subjects and in patients with unrepaired thoracic aortic diseases [5–10]. These studies share some consistent findings, for example, the ascending aorta experiences dramatic simultaneous longitudinal and diametric deformations, in conjunction with three-dimensional displacements. Recently, several studies have described pre- to post-TEVAR geometric changes including straightening of the descending thoracic aorta after endograft placement [11–13]. van Prehn et al. found a trend toward decreased diametric compliance of the thoracic aorta where the endograft was placed [14]. Nauta et al. and Hirotsu et al. added another interesting finding in which there was increased longitudinal strain proximal to the repaired thoracic aorta [15,16]. However, no studies have quantified full multiaxial deformation of the thoracic aorta before and after TEVAR.

The aim of this study is to propose methodology to quantify cardiac pulsatility-induced multiaxial deformation changes to the thoracic aorta from pre- to post-TEVAR using cardiac-gated computed tomography angiography (CTA) and custom geometric modeling techniques. The axial length, centerline and surface longitudinal curvatures, and cross-sections of the thoracic aorta during the cardiac cycle were analyzed in order to quantify both bulk and local deformations. This information will be essential for understanding the mechanical impact of TEVAR on the thoracic aorta, and may also assist in predicting long-term clinical outcomes of TEVAR.

2. Materials and methods

2.1. Study cohort and image acquisition

Patients from a single-institution who underwent descending aortic TEVAR to treat acute or chronic Type-B aortic dissections or chronic thoracic aortic aneurysm (recruited during July 2012 ~ March 2015) were selected for analysis based on having retrospective cardiac-gated CTA both before and after TEVAR [13]. Informed consent was obtained from each patient for image access, analysis, and publishing.

Retrospective use of images was approved by institutional review board with waiver of patient consent. Each patient underwent CTAs using either a single-source (LightSpeed VCT; GE Healthcare, Waukesha, WI) or a dual-source CT scanner (SOMATOM Definition; Siemens Healthcare, Erlangen, Germany). All CTAs were gated with retrospective electrocardiogram gating. Nonionic contrast medium was injected at a rate of 4−5 mL/s (Isovue 300 or 370, Bracco Diagnostics, Princeton, NJ). The tube potential was 120 kVp, field of view was $30 \times 30-40 \times 40$ cm^2, and axial slice thickness was 1.00–1.25 mm. The cardiac cycle was resolved to ten cardiac frames from 10 % to 100 % of the R-R interval, where 10 % corresponds to the beginning of systole and 100 % corresponds to the end of diastole. All CT scans utilized in this study were obtained as part of routine clinical care.

2.2. Computational modeling and centerline acquisition

Fig. 1 depicts the overall procedure of aortic modeling and extraction of centerline, inner and outer surface curve, as well as cross-sectional geometry. For each cardiac frame pre- and post-TEVAR, CTA images were processed using custom vascular modeling software (SimVascular, Open Source Medical Software Corp., San Diego, CA) [17–19]. First, paths of the aorta and adjacent branches were constructed along the lumen shown in CT images. Next, along the aortic path, the aortic lumen was orthogonally segmented from the aortic root to the distal descending aorta, using an automatic 2D level-set segmentation technique. In cases where the anatomy was severely tortuous, overlapping 2D contours were manually corrected by adjusting the contour spacing locally. From the segmented contours, mathematical centroids were computed. Then, the centroids were connected and smoothed with optimized Fourier smoothing to form an aortic centerline. Additionally, ostia of adjacent branches (coronary arteries, brachiocephalic artery, left common carotid artery, left subclavian artery, intercostal artery) were orthogonally segmented to be used as anatomic markers.

2.3. Identification of aortic segment and surface curves

In addition to the centerline, inner and outer surface curves of the thoracic aorta were extracted from the lumen contours such that they maintained consistent relative circumferential positions with respect to an arch branch vessel along the length of the aorta. Multiple longitudinal
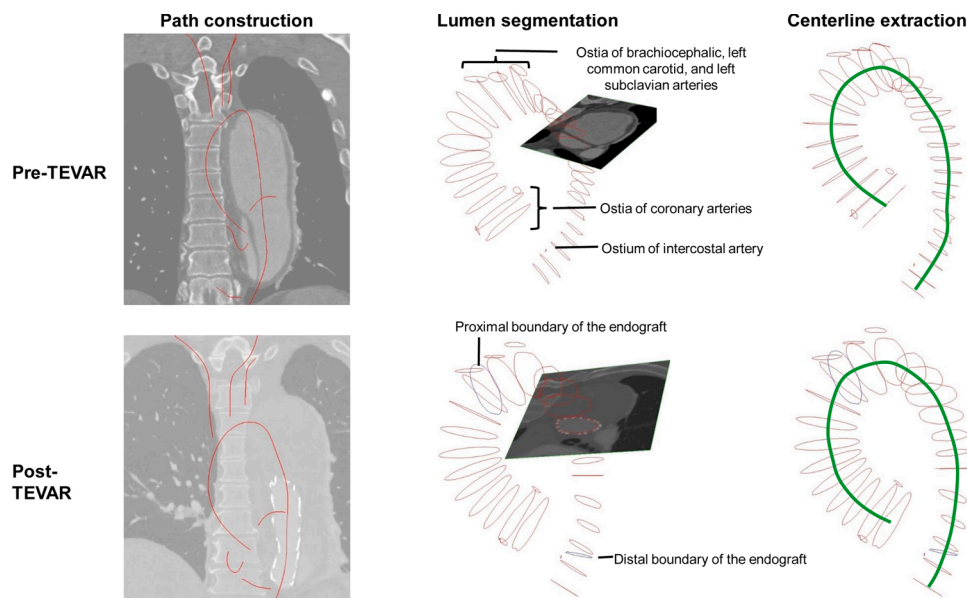
Fig. 1. CT-based lumen segmentation and centerline extraction for pre-TEVAR (top row) and post-TEVAR aorta (bottom row). Initial lumen path construction (left column), segmentation lumen contours, branch ostia, and endograft boundaries (middle column), and aortic centerline extraction (right column).

surface curves were formed along the surface of the aorta with respect to a fiducial guideline passing thee left common carotid ostia [20,21]. The inner surface curve was found by identifying the shortest longitudinal path along the surface of the aorta. The outer surface curve was formed by the lumen contour points that were separated 180 degrees from the inner surface curve points.

To quantify localized deformation of the thoracic aorta, two aortic segments were defined: ascending aorta and stented aorta (Fig. 2). The ascending aorta was defined from the ostium of the right coronary artery to the ostium of the brachiocephalic artery. The stented aorta was defined by the position of the endograft. Since the endograft was not present pre-TEVAR, longitudinal positions of the proximal and distal boundaries of the endograft post-TEVAR (with respect to adjacent branch vessels) were quantified and projected onto the native thoracic aorta in the pre-TEVAR state; this region was defined as the 'pre-TEVAR stented aorta'. For patients where the pre-TEVAR CTA field-of-view did not capture the location of the distal end of the post-TEVAR endograft, an alternative anatomic marker (intercostal artery ostia) present in both pre- and post-TEVAR images was used to define the distal boundary of the stented aorta.

2.4. Longitudinal, bending, and cross-sectional deformations

Geometric parameters for quantification of multiaxial pulsatile deformations in the ascending aorta and stented aorta included: 1) axial length of centerline (longitudinal deformation), 2) longitudinal curvatures of centerline, inner surface curve, and outer surface curve (bending deformation), and 3) effective diameter and eccentricity of lumen contours (cross-sectional deformation). All parameters were measured for all cardiac frames, and maximum deformations were quantified as the minimum-to-maximum percent changes. Centerline, inner surface curve, and outer surface curve curvature values were defined as the reciprocals of radii of curvature, where each circle was fit to three points along a curve: the point of interest, and proximal and distal points spanning 30 mm based on recommendations from previous studies [18, 21,22]. To ensure the use of a symmetric circle fitting with 15 mm on either side of the point of interest, the most proximal and distal 15 mm of the curve were omitted. To measure cross-sectional deformation, effective diameters of the ascending and stented aortas were calculated using the cross-sectional area of each segmented contour. Furthermore, eccentricity of the ascending and stented aortas were calculated using:

$$\varepsilon = \sqrt{1 - \left(\frac{b}{a}\right)^2}$$

where a and b represents the major and minor axis in each segmented contour, respectively.

2.5. Cardiac-resolved data presentation

Geometric quantification was performed for each of the ten cardiac frames for both pre- and post-TEVAR states, producing two types of data describing the change from pre- to post-TEVAR. First, time-averaged data indicates overall change from pre- to post-TEVAR. Second, amplitude data indicates damping (decrease) or augmentation (increase) in pulsatility from pre- to post-TEVAR. Statistical comparisons of geometric deformation were performed between pre- and post-TEVAR states. The two-tailed paired t-tests (differences in mean) and f-tests (differences in variance) were performed using MATLAB (MathWorks, Natick, MA). Significance threshold was set at a P value of 0.05.

3. Results

3.1. Patient demographics

This study included 11 patients (8 males and 3 females, age: 57–89) with four acute and five chronic Type B dissections, and two chronic thoracic aortic aneurysms, all of whom were treated with TEVAR. Patient demographics, device details, and time intervals between the pre- and post-TEVAR CTA acquisitions are shown in Table 1. The mean imaging interval between pre- and post-TEVAR was 302 ± 429 days (7–1518 days).

3.2. Longitudinal deformation

From pre- to post-TEVAR, the ascending aorta underwent a significant increase in arclength deformation during cardiac pulsation ($5.9 \pm 3.1\% \rightarrow 8.8 \pm 4.4\%$, $P < 0.05$). The stented aorta underwent a significant decrease in arclength deformation ($7.5 \pm 5.1\% \rightarrow 2.7 \pm 2.5\%$, $P < 0.05$).
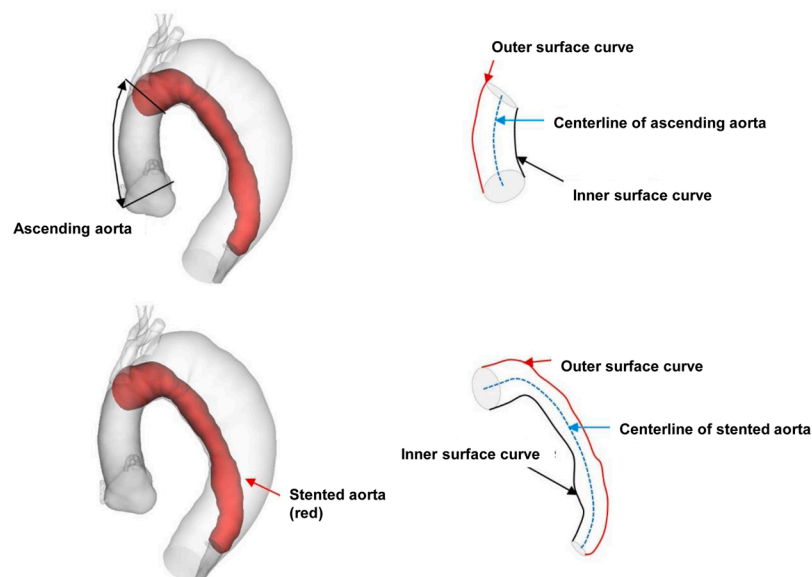

Fig. 2. Identification of ascending and stented aorta (post-TEVAR) (left column), and representation of centerline, inner surface, and outer surface curves for ascending and stented aorta (right column).

Table 1

Patient demographics and TEVAR-specific information.

Patient	Age (years)	Sex (M/ F)	Disease (Dissection/ Aneurysm)	Device information (diameter × length cm, Gore C-TAG except where noted)	Imaging interval between pre- and post- TEVAR (days)
1	69	M	Dissection	4.0 × 20.0	50
2	57	M	Dissection	3.4 × 20.0	302
3	82	M	Dissection	3.4 × 20.0	113
4	63	M	Dissection	3.4 × 20.0	372
5	68	M	Dissection	3.4 × 15.0 (proximal) 4.0 × 15.0 (distal)	214
6	58	M	Dissection	4.5 × 10.0 (proximal) 4.0 × 15.0 (middle) 3.4 × 20.0 (distal)	64
7	89	M	Aneurysm	3.7 × 10.0 (proximal) 3.7 × 10.0 (distal)	23
8	58	F	Dissection	3.1 × 15.0	7
9	75	F	Dissection	3.4 × 15.0 (proximal) 3.8 × 12.7 (middle, COOK) 4.2 × 13.5 (distal, COOK)	439
10	68	M	Dissection	3.4 × 20.2 (proximal, COOK) 3.8 × 20.2 (distal, COOK)	1518
11	69	F	Aneurysm	3.7 × 10.0 (proximal) 4.0 × 15.0 (middle) 4.5 × 20.0 (distal)	225

3.3. Cross-sectional and bending deformation

Fig. 3 depicts an example case (effective diameter of the native ascending aorta of Patient 1, pre- and post-TEVAR) with point-wise data plotted for all cardiac frames (10–100 % of R-R interval) over a normalized arclength (0–1). The time-averaged and amplitude plots represent average and time-varying changes to effective diameter, respectively, at each arclength position. Patient 1 exhibited an increase of time-averaged ascending aortic effective diameter from pre- to post-TEVAR, except at the ends close to branch vessels. Furthermore, the amplitude of effective diameter was increased from pre- to post-TEVAR after the first quarter of arclength. This means that after TEVAR, the ascending aorta was enlarged in the mid-section and its pulsatile diametric distension increased.

As demonstrated in Patient 1, multiaxial deformation of the stented aorta and ascending aorta were quantified for all patients. Fig. 4 depicts time-averaged and amplitude plots of 11 patients for inner surface curvature, centerline curvature, outer surface curvature, effective diameter, and cross-sectional eccentricity of the stented aorta. Amplitudes of inner surface, centerline, and outer surface curvature were significantly decreased along the arclength from pre- to post-TEVAR. In addition, both time-averaged and amplitude of effective diameter were significantly decreased along the proximal endograft from pre- to post-TEVAR. Eccentricity was not statistically different between pre- and post-TEVAR.

Fig. 5 depicts time-averaged and amplitude plots of 11 patients for inner surface curvature, centerline curvature, outer surface curvature, effective diameter, and cross-sectional eccentricity of the ascending aorta. Amplitudes of inner surface curvature and centerline curvature were increased from pre- to post-TEVAR along the distal portion of the ascending aorta close to the brachiocephalic ostium, also accompanied
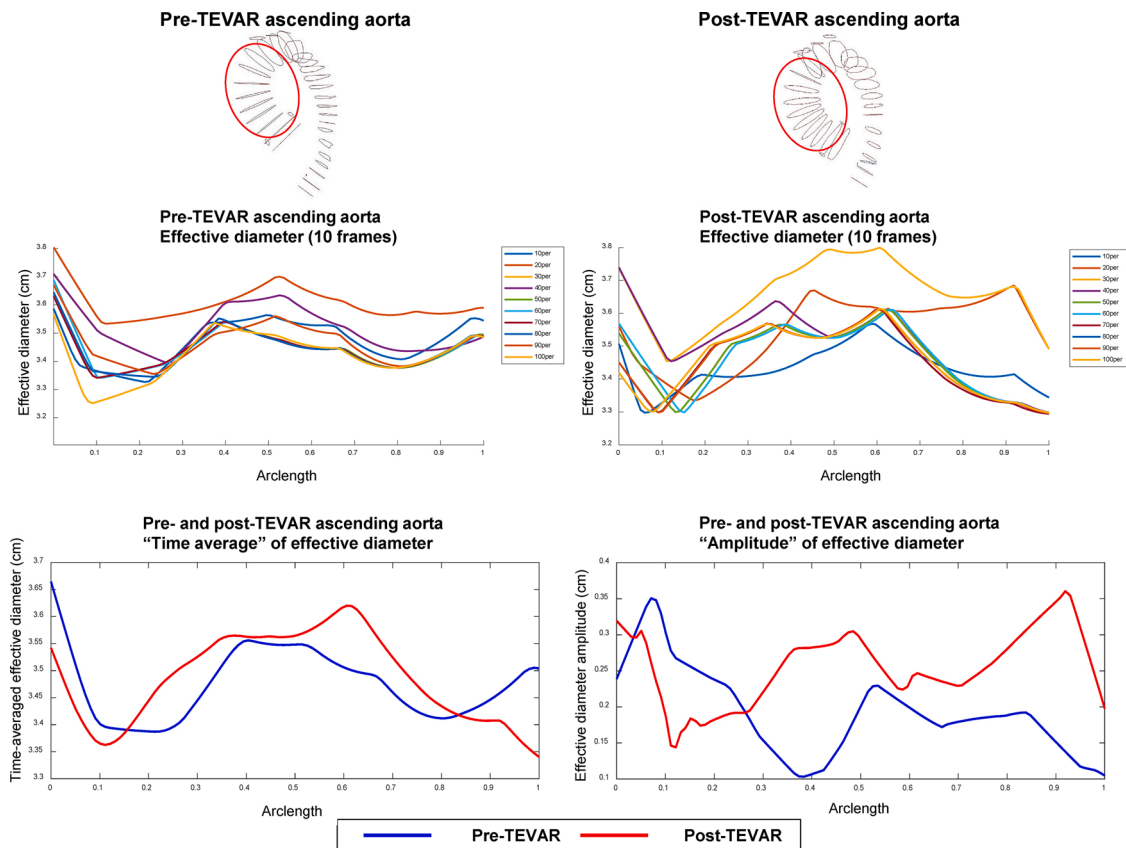
Fig. 3. Representative ascending aortic effective diameter data for Patient 1, pre- and post-TEVAR, plotted against normalized length. Point-wise effective diameter was quantified along the ascending aorta for 10 cardiac frames (middle row). Ten-frame data was merged in two types of representation (bottom row): time average (the average of ten-frame measurements) and amplitude (the maximum difference during the ten cardiac frames).

Geometric parameters

Stented aorta (average of 11 patients)
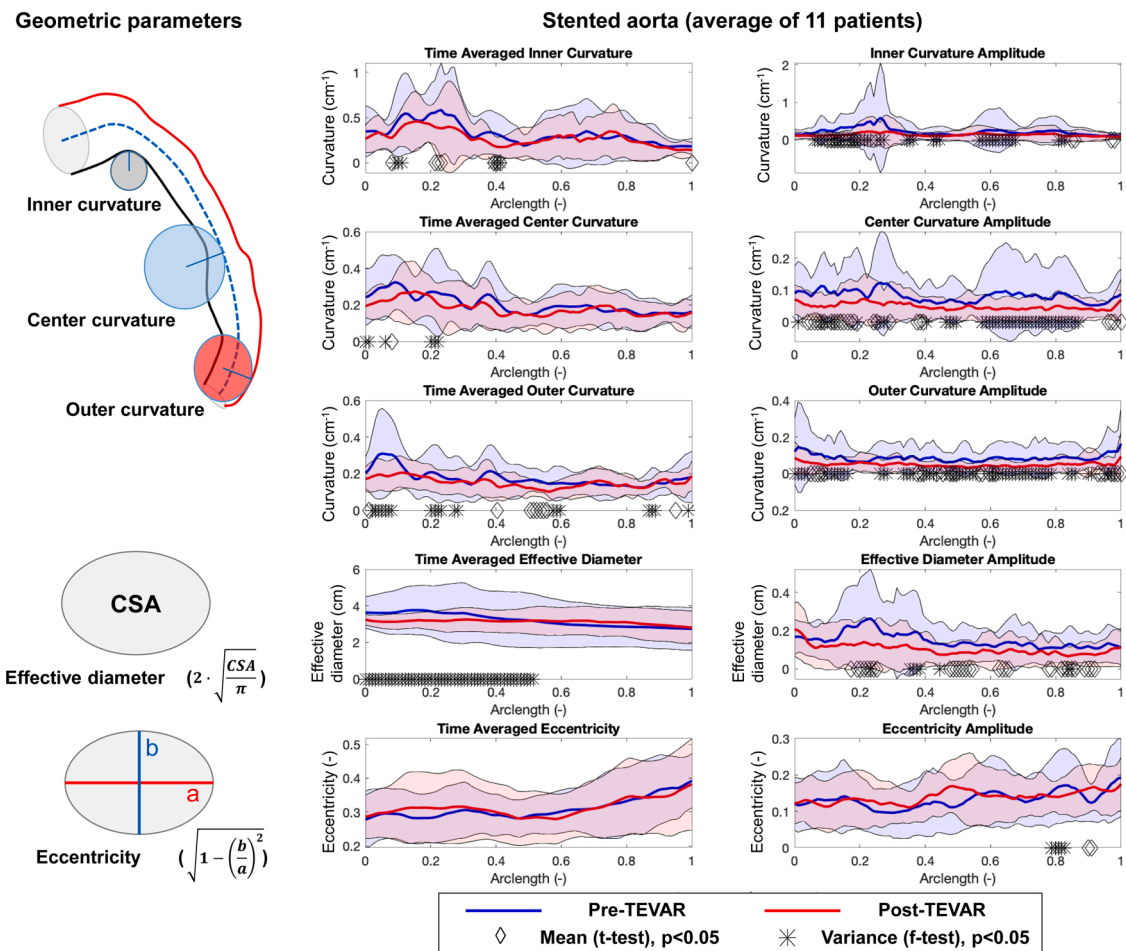
Fig. 4. Graphical definitions of each geometric parameter for the stented aorta are shown in the left column. Time-averaged (middle column) and amplitude plots (right column) of 11 patients representing inner surface curvature, centerline curvature, outer surface curvature, effective diameter (calculated from cross-sectional area (CSA)), and cross-sectional eccentricity of the stented aorta (solid thick line: average, shaded regions: standard deviation). Point-wise pre- vs. post-TEVAR *t*-test and f-test comparisons are shown on the x-axis for each parameter.

by higher variance. The amplitude of eccentricity was increased from pre- to post-TEVAR along the distal portion of the ascending aorta. There were no consistent pre-to-post-TEVAR differences in outer curvature or effective diameter.

4. Discussion

4.1. Multi-axial deformation of the stented aorta

The stented descending aorta experienced significantly decreased deformation in axial length (~65 % decrease), accompanied by reduced amplitude of centerline and surface curvatures (~40 % decrease) and effective diameter (~30 % decrease) during the cardiac cycle. Muted deformation in the longitudinal, bending, and cross-sectional directions within the stented region is a result of the endograft and tissue remodeling adding stiffness in all directions, which reduces pulsatile compliance of the stented aorta. For example, the substantial reduction of amplitude of the inner surface, centerline, and outer surface curvatures of the stented aorta along the entire stented region reveals the strong damping of local bending deformation. Endografts are designed to be flexible in the bending direction with Nitinol stents covered with soft graft material; this enables the endograft to be conformable during implantation. However, after tissue incorporation, the TEVAR-treated descending aorta stiffens and damps pulsatile motion in the longitudinal, bending, and cross-sectional directions.

4.2. Multi-axial deformation of the ascending aorta

TEVAR induced significant changes in pulsatile deformations not only in the stented aorta but also in the ascending aorta. From pre- to post-TEVAR, the ascending aorta experienced increased axial length deformation by approximately 50 %. At the same time, the distal ascending aorta near the aortic arch exhibited increased amplitudes of inner surface and centerline curvatures, accompanied by increased amplitude of cross-sectional eccentricity. The main driving force of ascending aortic deformation is the left ventricular contraction for both pre- and post-TEVAR states. This pre-to-post-TEVAR amplification of aortic axial deformation suggests amplified wave reflection from the stiffened distal stented aorta. Furthermore, the ascending aorta must accommodate the decreased bending compliance of the stented descending aorta, and may lead to enhanced bending with collapsed cross-section near the aortic arch [16]. The increase in strain proximal to the endograft evokes the classic experiment performed by Baron et al., where artificial aortic coarctation in monkeys caused increased strain proximal to the coarctation and precipitated atherosclerotic disease progression [23].

4.3. Comparison with the previous studies

Our findings are consistent with those found in other cardiac pulsatility-induced deformation studies of the thoracic aorta.

Based on our findings, axial strains for the ascending aorta were

Geometric parameters   **Ascending aorta (average of 11 patients)**
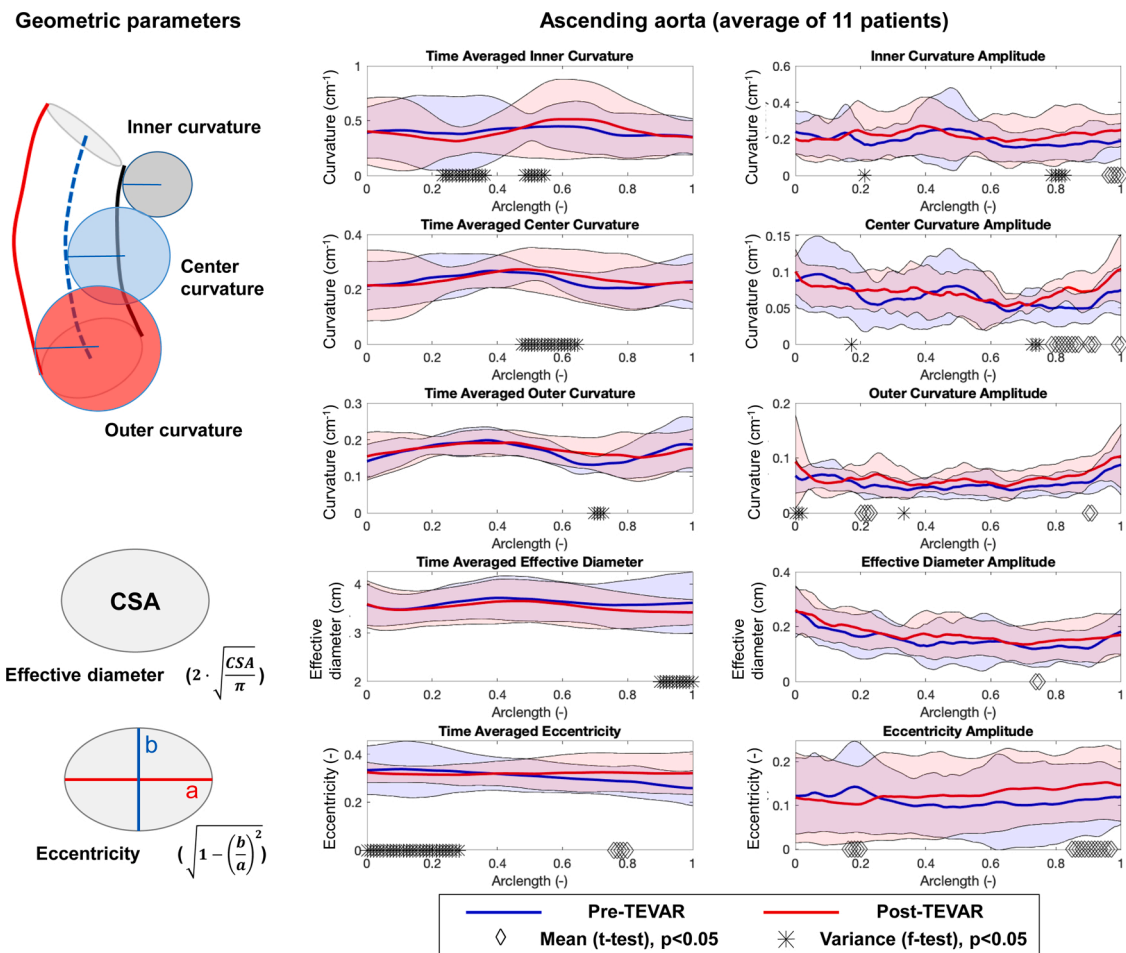
Fig. 5. Graphical definitions of each geometric parameter for the ascending aorta are shown in the left column. Time-averaged (middle column) and amplitude plots (right column) of 11 patients representing inner surface curvature, centerline curvature, outer surface curvature, effective diameter (calculated from cross-sectional area (CSA)), and cross-sectional eccentricity of the ascending aorta (solid thick line: average, shaded regions: standard deviation). Point-wise pre- vs. post-TEVAR *t*-test and f-test comparisons are shown on the x-axis for each parameter.

5.9 ± 3.1 % and 8.8 ± 4.4 %, pre-TEVAR and post-TEVAR, respectively. Axial strains for the stented aorta were 7.5 ± 5.1 % and 2.7 ± 2.5 %, pre-TEVAR and post-TEVAR, respectively. Nauta et al. reported axial strain data for two patients with type B aortic dissection at pre- vs. post-TEVAR states, and the axial strain in the ascending aorta was 5.0 % vs. 5.3 % in patient 1 and 9.9 % vs. 16.8 % in patient 2, and in the descending aorta was 1.5 % vs. 2.4 % in patient 1 and 4.9 % vs. 1.7 % in patient 2 [15]. These values fall within the range of deformations reported in this study, with the exception of the higher axial strain of the ascending aorta in patient 2 from Nauta et al. Note that this patient had a history of Marfan's syndrome and ruptured Type-B aortic dissection at age younger than 60 years. de Beaufort et al. studied pulsatile aortic deformation of patients with thoracic aortic aneurysms pre- and post-TEVAR, and reported that the axial strain changed from 7.1 % to 15.3 % for the ascending aorta and from 1.2 % to 3.8 % for the descending aorta [10]. The same study showed changes in diametric strain from 5.0 % to 6.3 % for the ascending aorta from pre- to post-TEVAR, which are also well within the range of our findings. The increased deformation in the ascending aorta post-TEVAR may be related to the clinical findings of increased rate of ascending aortic enlargement and left ventricular remodeling observed during post-TEVAR follow-up [24,25].

For our cohort, diametric strains averaged within the ascending aorta were 3.5 ± 1.5 % and 4.0 ± 1.6 %, pre-TEVAR and post-TEVAR, respectively. Diametric strains averaged within the stented aorta were 3.3 ± 2.3 % and 1.8 ± 1.3 %, pre-TEVAR and post-TEVAR, respectively. Morrison et al. studied aging effect on cardiac deformability of the

thoracic aorta dividing 14 healthy subjects into a younger (mean age, 41 years) and older group (mean age, 68 years) [5]. Older group exhibited cyclic diametric strain from 2.5 ± 1.2 % to 3.4 ± 1.5 % for the ascending aorta, and from 2.0 ± 2.0 % to 4.2 ± 1.9 % for the descending aorta. Our pre-TEVAR diametric strains agreed well with the results of Morrison et al.

In contrast to our study, none of these preliminary studies performed extensive analysis reviewing all cardiac frames, comparing pre- and post-TEVAR, computing longitudinal, cross-sectional, and bending deformations of regions defined by material points.

4.4. Importance of multi-axial geometric quantification

Quantification of cross-sectional, axial, and bending deformations enables a full understanding of the biomechanical motions the aorta and implanted endografts. This provides information critical not only for device durability evaluation, but also aids in our understanding of how TEVAR impacts the multiaxial biomechanics of the thoracic aorta. For example, pre- and post-TEVAR deformations provide deformation damping (at the site of the endograft) and augmentation (at adjacent native sites) factors, which can be used for product development of devices placed initially, as well as those implanted subsequently. In addition, quantification of inner and outer surface curvatures, a unique feature of the methods presented in this study, provides additional geometric information that centerline-based methods cannot capture [18,19]. The presence of high inner surface curvatures at the proximal

landing zone may increase the risk of endograft mal-apposition and Type 1a endoleak, thus surface curvatures may be useful for guiding implantation strategy [26–29].

4.5. Limitations

The patient cohort exhibited variability in disease etiology, endograft coverage, and number of endografts employed for TEVAR. This was due to the limited number of patients who met the inclusion criteria of having full retrospective cardiac-gated CTA for pre- and post-TEVAR. As this study was not intended to add any study-driven imaging with radiation to study participants, we reviewed participants' medical record to search for eligible CTAs retrospectively. In the case of Patient 10, for example, the imaging interval between pre- and post-TEVAR was 1518 days since the CTAs at intermediate time points were non-gated and not eligible for study analysis. Variability in pre-to-post-TEVAR imaging interval means that there could be different amounts of post-op healing and remodeling in the cohort. Blood pressure and other hemodynamic measurements were not required for inclusion into this study, which limited true compliance quantification (distension per 100 mmHg) and investigation of the impact of TEVAR on hemodynamics and vice versa. For example, it is possible that acute reduction of wall compliance due to TEVAR may result in augmented blood pressure [30]. Acquisition of blood pressure pre- and post-TEVAR, along with computational flow simulations, could help with hemodynamics investigations in future studies. This study did not consider the potential effect of calcification on the deformation of the thoracic aorta. Based on previous studies, we opine that highly calcified regions (mostly in the descending aorta) undergo less cardiac-induced deformation than non-calcified regions, which result in less change of deformation due to TEVAR [31]. This study did not investigate the differences between different endograft designs, or include the dynamics of the aortic arch, which is an important region to consider in the context of branched TEVAR. Expansion of the patient cohort and more comprehensive investigation on aortic remodeling via multiple follow-up time points after TEVAR are warranted. Finally, reproducibility of the measurements may be improved with fully-automated geometric modeling. While quantification and analytic methods were fully automated, image-based modeling involved some manual components, which may contribute to operator-driven variability.

5. Conclusions

The thoracic aorta exhibits complex, time-dependent multiaxial deformations, and TEVAR alters these deformations dramatically. The stented aorta experiences decreased deformation in all directions due to stiffening of the aorta, while the ascending aorta experiences increased deformation to compensate for the reduced compliance in the stiffened stented aorta. The present work provides essential information to understand the mechanical impact of TEVAR on cardiac pulsatility-induced *in vivo* motion, which is critical for surveillance of long-term outcomes of TEVAR, as well as future product development.

Presentation information

Preliminary outcomes of this study was presented at Leipzig Interventional Course (LINC), Leipzig, Germany, Jan. 30th – Feb 2nd, 2018.

Ethical statement

- This research study is the authors' own original work, which has not been previously published elsewhere.
- The manuscript is not currently being considered for publication elsewhere.
- The manuscript reflects the authors' own research and analysis in a truthful and complete manner.

- The manuscript properly credits the meaningful contributions of co-authors.
- All authors have been personally and actively involved in substantial work leading to the paper, and will take public responsibility for its content.
- The study results are appropriately placed in the context of prior and existing research.
- As this study involved the use of human subjects, this study was carried out in accordance with The Code of Ethics of the World Medical Association, and a statement is included in the manuscript that informed consent was obtained for this study.
- All sources used are properly disclosed. Literally copying of text must by indicated as such by quotation marks and giving proper reference.

CRediT authorship contribution statement

Ga-Young Suh: Conceptualization, Methodology, Software, Writing - original draft, Project administration. **Johan Bondesson:** Software, Validation, Formal analysis, Visualization, Writing - review & editing. **Yufei D. Zhu:** Methodology, Software, Writing - review & editing. **Jason T. Lee:** Conceptualization, Methodology, Investigation, Resources. **Michael D. Dake:** Conceptualization, Writing - review & editing, Resources. **Christopher P. Cheng:** Conceptualization, Supervision, Writing - review & editing, Funding acquisition, Project administration.

Declaration of Competing Interest

The authors declare the following financial interests/personal relationships which may be considered as potential competing interests:

GS is a consultant for W. L. Gore & Associates and Terumo. CPC is a consultant for W. L. Gore & Associates, Terumo, and Endospan. MDD is a consultant for W. L. Gore & Associates and Cook Medical. JB, YDZ, and JTL have nothing to disclose.

References

[1] J.E. Bavaria, J.J. Appoo, M.S. Makaroun, et al., Endovascular stent grafting versus open surgical repair of descending thoracic aortic aneurysms in low-risk patients: a multicenter comparative trial, J. Thorac. Cardiovasc. Surg. 133 (2007) 369–377.

[2] C.J. Beller, M.R. Labrosse, M.J. Thubrikar, et al., Role of aortic root motion in the pathogenesis of aortic dissection, Circulation 109 (2004) 763–769.

[3] D. Cheng, J. Martin, H. Shennib, et al., Endovascular aortic repair versus open surgical repair for descending thoracic aortic disease: a systemic review and meta-analysis of comparative studies, J. Am. Coll. Cardiol. 55 (2010) 986–1001.

[4] U. Raaz, A.M. Zollner, I.N. Schellinger, et al., Segmental aortic stiffening contributes to experimental abdominal aortic aneurysm development, Circulation 131 (2015) 1783–1795.

[5] T.M. Morrison, G. Choi, C.K. Zarins, et al., Circumferential and longitudinal cyclic strain of the human thoracic aorta: age-related changes, J. Vasc. Surg. 49 (2009) 1029–1036.

[6] G.Y. Suh, R.E. Beygui, D. Fleischmann, et al., Aortic arch vessel geometries and deformations in patients with thoracic aortic aneurysms and dissections, J. Vasc. Interv. Radiol. 25 (2014) 1903–1911.

[7] F. Rengier, T.F. Weber, V. Henninger, et al., Heartbeat-related distension and displacement of the thoracic aorta in healthy volunteers, Eur. J. Radiol. 81 (2012) 158–164.

[8] T.F. Weber, M.K. Ganten, D. Bockler, et al., Heartbeat-related displacement of the thoracic aorta in patients with chronic aortic dissection type B: quantification by dynamic CTA, Eur. J. Radiol. 72 (2009) 483–488.

[9] K. Emilsson, R. Egerlid, B.M. Nygren, Comparison between aortic annulus motion and mitral annulus motion obtained using echocardiography, Clin. Physiol. Funct. Imaging 26 (2006) 257–262.

[10] H.W.L. de Beaufort, F.J.H. Nauta, M. Conti, et al., Extensibility and distensibility of the thoracic aorta in patients with aneurysm, Eur. J. Vasc. Endovasc. Surg. 53 (2017) 199–205.

[11] M. Midulla, R. Moreno, A. Negre-Salvayre, et al., Impact of endografting on the thoracic aortic anatomy: comparative analysis of the aortic geometry before and after the endograft implantation, Cardiovasc. Interv. Radiol. 37 (2014) 69–76.

[12] G. Mestres, M.E. Garcia, X. Yugueros, et al., Aortic arch and thoracic aorta curvature remodeling after thoracic endovascular aortic repair, Ann. Vasc. Surg. 38 (2017) 233–241.

[13] B.W. Ullery, G.Y. Suh, K. Hirotsu, et al., Geometric deformations of the thoracic aorta and supra-aortic arch branch vessels following thoracic endovascular aortic repair, Vasc. Endovasc. Surg. 52 (2018) 173–180.

[14] J. van Prehn, L.W. Bartels, G. Mestres, et al., Dynamic aortic changes in patients with thoracic aortic aneurysms evaluated with electrocardiography-triggered computed tomographic angiography before and after thoracic endovascular aneurysm repair: preliminary results, Ann. Vasc. Surg. 23 (2009) 291–297.

[15] F. Nauta, G. van Bogerijen, M. Conti, et al., Impact of thoracic endovascular repair on pulsatile aortic strain in acute type B aortic dissection, Aorta 5 (2017) 42–52.

[16] K. Hirotsu, G. Suh, J.T. Lee, et al., Changes in geometry and cardiac deformation of the thoracic aorta after thoracic endovascular aortic repair, Ann. Vasc. Surg. 46 (2018) 83–89.

[17] N. Wilson, K. Wang, R.W. Dutton, et al., A software framework for creating patient specific geometric models from medical imaging data for simulation based medical planning of vascular surgery, Lect. Notes Comput. Sci. 2208 (2001) 449–456.

[18] G. Choi, C.P. Cheng, N.M. Wilson, et al., Methods for quantifying three-dimensional deformation of arteries due to pulsatile and nonpulsatile forces: implications for the design of stents and stent grafts, Ann. Biomed. Eng. 37 (2009) 14–33.

[19] G.Y. Suh, B.W. Ullery, J.T. Lee, et al., Cardiopulmonary-induced deformations of the thoracic aorta following thoracic endovascular aortic repair, Vascular (2018), https://doi.org/10.1177/1708538118811204.

[20] J. Bondesson, G.Y. Suh, T. Lundh, et al., Automated quantification of diseased thoracic aortic longitudinal centerline and surface curvatures, J Biomech. Eng. 142 (2020) 041007.

[21] T. Lundh, G.Y. Suh, P. DiGiacomo, et al., A lagrangian cylindrical coordinate system for characterizing dynamic surface geometry of tubular anatomic structures, Med. Biol. Eng. Comput. 56 (2018) 1659–1668.

[22] C.P. Cheng, Y.D. Zhu, G.Y. Suh, Optimization of three-dimensional modeling for geometric precision and efficiency for healthy and diseased aortas, Comput. Methods Biomech. Biomed. Eng. 21 (2018) 65–74.

[23] B.W. Baron, S. Glagov, D.P. Giddens, et al., Effect of coarctation on matrix content of experimental aortic atherosclerosis: relation to location, plaque size and blood pressure, Atherosclerosis 102 (1993) 37–49.

[24] T. Hiraoka, T. Komiya, T. Shimamoto, Enlargement rate of the ascending aorta after thoracic endovascular aortic repair, Semin. Thorac. Cardiovasc. Surg. (2019), https://doi.org/10.1053/j.semtcvs.2019.09.010.

[25] P. Vallerio, A. Maloberti, I. D'Alessio, et al., Cardiovascular remodeling after endovascular treatment for thoracic aortic injury, Ann. Vasc. Surg. (2019), https://doi.org/10.1016/j.avsg.2019.04.015.

[26] D. Kotelis, C. Brenke, S. Wörz, et al., Aortic morphometry at endograft position as assessed by 3D image analysis affects risk of type I endoleak formation after TEVAR, Langenbecks Arch. Surg. 400 (2015) 523–529.

[27] T. Kudo, T. Kuratani, K. Shimamura, et al., Type 1a endoleak following Zone 1 and Zone 2 thoracic endovascular aortic repair: effect of bird-beak configuration, Eur. J. Cardiothoracic Surg. 52 (2017) 718–724.

[28] M. Boufi, C. Guivier-Curien, V. Deplano, et al., Risk factor analysis of bird beak occurrence after thoracic endovascular aortic repair, Eur. J. Vasc. Endovasc. Surg. 50 (2015) 37–43.

[29] M.M. Frohlich, G.Y. Suh, J. Bondesson, et al., Aortic geometry correlates with endograft bird-beaking severity, J. Vasc. Surg. 72 (2019) 1196–1205.

[30] C.V. Ioannou, N. Stergiopulos, A.N. Katsamouris, et al., Hemodynamics induced after acute reduction of proximal thoracic aorta compliance, Eur. J. Vasc. Endovasc. Surg. 26 (2003) 195–204.

[31] M.M. Ahmad, S.H.A. Pir, M.N. Muhammad, et al., Influence of differential calcification in the descending thoracic aorta on aortic pulse pressure, J. Patient. Res. Rev. 4 (2017) 104–113.